Available online at www.sciencedirect.com
SCIENCE DIRECT®
International Journal of Mass Spectrometry 245 (2005) 14–25
International Journal of Mass Spectrometry
www.elsevier.com/locate/ijms

Review

Rovibronic photoionization dynamics of asymmetric-top molecules

S. Willitsch[a], F. Merkt[b,*]

[a] *Department of Chemistry, University of Oxford, Chemistry Research Laboratory, Mansfield Road, Oxford OX1 3TA, UK*
[b] *Physical Chemistry, ETH Zurich, 8093 Zurich, Switzerland*

Received 2 May 2005; accepted 20 June 2005
Available online 26 July 2005

Abstract

Recent progress in the study of the rovibronic photoionization dynamics of polyatomic molecules is reviewed with emphasis on the photoionization dynamics of asymmetric tops. Rovibronic photoionization selection rules and propensities for angular momentum transfer upon photoionization are discussed in the framework of an orbital ionization model in which the ionization is assumed to take place out of a single determinantal electronic wavefunction. This model enables the quantitative analysis of the rotational structure of photoelectron spectra whenever the photoionization can be interpreted in a single-determinantal picture. In more complicated situations, the model can be used to identify configurational mixing in the neutral or the cationic state and to detect rovibronic interactions between the ionization channels. Various aspects of the model are illustrated by examples including studies of the photoionization and photoelectron spectra of ketene (CH_2CO), ozone (O_3), ethylene (C_2H_4) and amidogen (NH_2).

Keywords: Photoionization; Photoelectron spectroscopy; High Rydberg states; ZEKE; Molecular cations

Contents

1. Introduction

Photoionization represents a powerful method for the generation of molecular cations and is used in many analytical and spectroscopic applications such as mass spectrometry, photoionization spectroscopy, resonance-enhanced multiphoton-ionization (REMPI) spectroscopy and photoelectron spectroscopy. Whereas the dynamical details of the ionization process are only of secondary importance in mass spectrometric studies, the production of the cations and

* Corresponding author.
E-mail address: frederic.merkt@ethz.ch (F. Merkt).

1387-3806/$ – see front matter © 2005 Elsevier B.V. All rights reserved.
doi:10.1016/j.ijms.2005.06.004

their subsequent mass analysis being usually at the center of interest, the photoionization dynamics is a key aspect of the spectroscopic applications of photoionization: It determines which quantum states of the cation can be produced or studied from a given quantum state of the parent neutral species and governs the intensity distribution of photoelectron spectra [1–4]. A detailed understanding of the photoionization process is therefore important for the production of state-selected molecular cations which is a prerequisite for the study of state-selected ion–molecule reactions [5–9].

The investigation of the rovibronic photoionization dynamics of a wide range of polyatomic molecules by photoelectron spectroscopic methods has become possible with the development of pulsed-field-ionization zero-kinetic-energy (PFI-ZEKE) photoelectron spectroscopy [10–17]. In conventional photoelectron spectroscopy, the molecules are ionized with radiation of a fixed frequency and the photoelectron kinetic energy, which corresponds to the difference between the photon energy and the internal energy of the cationic core, is measured [18]. In contrast, in PFI-ZEKE photoelectron spectroscopy the parent neutral molecules are excited with a tunable light source to very high Rydberg states located just below the ionization thresholds associated with the accessible quantum states of the cation. The high Rydberg states (with principal quantum numbers $n \gtrapprox 100$) are ionized by electric field pulses and the field ionization yield is recorded as a function of the excitation energy to give the PFI-ZEKE photoelectron spectrum [10,13,19]. In this way, a spectral resolution of better than $1\,\mathrm{cm}^{-1}$ can be routinely achieved which is sufficient to resolve the rovibronic structure of many diatomic and symmetric polyatomic molecules.

The majority of polyatomic molecules, however, exhibits low symmetry, have three distinct rotational constants and are thus asymmetric-top molecules. Because of the low symmetry, the density of non-degenerate rotational states is much higher in asymmetric-top than in symmetric-top molecules. Moreover, the photoionization symmetry selection rules are usually less restrictive, and resolving the rotational structure in the photoelectron spectra of asymmetric tops is notoriously difficult, particularly for molecules with small rotational constants. The experimental data on the rovibronic photoionization dynamics of asymmetric tops has therefore remained scarce up to date, the main exceptions being the triatomic hydrides H_2O [20–27], H_2S [28–30], CH_2 [31,32] and NH_2 [33] and formaldehyde H_2CO [34] which all have unusually large rotational constants. Partially resolved rotational contours have been analyzed in the photoelectron spectra of larger asymmetric tops such as, for instance, fluorobenzene [35] and *n*-butylbenzene [36]. The recent improvement of the resolution of PFI-ZEKE photoelectron spectroscopy to better than $0.1\,\mathrm{cm}^{-1}$ [19] enabled the observation of the rovibronic structure in the spectra of a wider range of asymmetric tops such as CH_2CO [37,38], C_2H_4 [39,40] and O_3 [41].

The growing body of experimental data on the rovibrational structure of photoelectron spectra of asymmetric-top molecules enables and justifies a discussion of the underlying photoionization dynamics, and we review in this article recent progress in the study of their photoionization dynamics. Rotationally resolved PFI-ZEKE photoelectron spectra are analyzed in the framework of a theoretical model [39,42] for the rovibronic photoionization intensities of asymmetric tops which is an extension of the model developed by Buckingham et al. for diatomic molecules [1]. This model has been at the heart of most approaches followed to date to calculate the rovibronic structure of photoelectron spectra ab initio [43–47]. Two aspects of the model particularly attractive for the chemist and central to the present article are that (i) it links the rotational structure of the photoelectron bands to the properties of the molecular orbital from which ionization occurs and (ii) it highlights the relationship between the photoionization dynamics of the molecule and the internal molecular dynamics of the cation core.

The main features of the model are best illustrated with the example of the photoionization of H_2 [48]. Removing an electron from the 1s σ_g orbital leads to the formation of the $\tilde{X}^+\,^2\Sigma_g^+$ H_2^+ ion and can be viewed as the creation of a (1s σ_g) hole in the core. By assuming that the angular momentum characteristics of the photoionizing radiation is fully transferred to the photoelectron, the conservation of angular momentum requires the vector addition of the ion total angular momentum without spin $\vec{N}^+$ and the electron hole angular momentum $\vec{\ell}''$ to be equal to that of the neutral molecule $\vec{N}''$ prior to ionization:

$$\vec{\ell}'' + \vec{N}^+ = \vec{N}''. \tag{1}$$

The (1s σ_g) orbital of H_2 can be viewed as an ℓ''=0 orbital centered halfway between the two protons, with only a very weak $\ell'' = 2$ contribution. Eq. (1) thus predicts that the main rotational branches of the photoelectron spectrum are a dominant $N^+ - N'' = 0$ branch and weaker $|N^+ - N''| = 2$ branches as confirmed by experiment [49–51]. This orbital approximation also enables one to predict, in this case, that the angular distribution of the photoelectron should be very similar to that expected following photoionization out of an s orbital of an atom. This prediction is also confirmed by angle-resolved photoionization experiments on H_2 molecules [52].

The orbital approximation outlined here is not suitable to describe the energy dependence of the photoionization dynamics and fails to describe the effects of shape resonances and Cooper minima on the rotational structure of photoelectron spectra [53–57]. It does, however, provide a useful framework to discuss rotational intensities in photoelectron spectra: it assists in the assignment of vibronic symmetries, it enables one to detect anomalies in the photoionization dynamics and it helps to reveal vibronic interactions in the molecular cations. These aspects are at the focus of this article, and examples will be presented in Section 5 illustrating each point.

2. Rovibronic photoionization selection rules and intensities

Photoionization entails an electronic transition between a bound and a continuum state. The main difficulty in the formulation of a model for rovibronic photoionization intensities lies in the treatment of the photoelectron which, in the asymptotic range, is only weakly coupled to the cationic core. In PFI-ZEKE photoelectron spectroscopy, the molecules are excited to a pseudo-continuum of very high Rydberg states in which the electron is weakly bound. In diatomic molecules, the transition can usually be described as occurring between a Hund's case (a) or (b) type angular momentum coupling situation in the initial state and a type (d) coupling situation in the final state. The absorption cross section varies smoothly through the ionization thresholds [58] so that intensity models for direct photoionization can equally well be applied to transitions to the pseudo-continua of very high Rydberg states that are probed in PFI-ZEKE photoelectron spectroscopic experiments, provided that the coupling between the different ionization channels are adequately taken into account [12,59,60].

In a single-determinantal description of photoionization, the wavefunction of the final state of the transition φ_f can be factorized into $\varphi_f = \varphi_{e^-}\varphi^+$ where φ_{e^-} and φ^+ stand for the wavefunctions of the photoelectron at long range and of the cation core, respectively. φ_{e^-} can be determined by solving the corresponding scattering equation (see, e.g., Ref. [45]) or using multichannel quantum defect theory (MQDT) [61–64]. The differential photoionization cross section of an isotropic (non-aligned, non-oriented) sample can be formulated as [1,65]

$$\frac{d\sigma_{tot}}{d\Omega} = \frac{\sigma_{tot}}{4\pi}(1 + \beta P_2(\cos\theta)) \propto \sum |\langle\varphi_{e^-}|\langle\varphi^+|\vec{\mu}|\varphi_i\rangle|^2. \quad (2)$$

In Eq. (2), σ_{tot} is the total photoionization cross section, $d\Omega$ the infinitesimal solid-angle element, P_2 the second-order Legendre polynomial and the sum runs over all degenerate initial and final states. By suitable modifications, Eq. (2) can also be extended to calculate differential and integral photoionization cross sections of aligned and oriented samples [66–69].

For the analysis of the molecular photoionization dynamics, Eq. (2) can be used to numerically calculate photoionization intensities or to derive photoionization selection rules. The evaluation of Eq. (2) was used by Dixit and McKoy [70] and Xie and Zare [71] to derive rovibronic photoionization selection rules for diatomic molecules. A similar approach was followed by Lee et al. to determine selection rules for the photoionization of H_2O [23]. A method to derive rovibronic selection and propensity rules for transitions to high Rydberg states which is in principle generally applicable to polyatomic molecules was introduced in the form of the "compound state model" by Müller-Dethlefs [72]. In this model, the wavefunctions of the Rydberg electron in the close-coupling and asymptotic regimes are correlated diagrammatically and photoionization selection and propensity rules are derived from the correlation diagrams. The model offers the advantage of providing some information on relative intensities, but the construction of the correlation diagrams can prove laborious in practical situations. The model has been applied in the analysis of the photoionization of NO, H_2S, N_2O and NH_3 [30,72].

The most general set of rovibronic photoionization selection rules is obtained by invoking the conservation of parity and nuclear spin symmetry, resulting in the symmetry condition [73]

$$\Gamma_{e^-} \otimes \Gamma^+_{rve} \otimes \Gamma''_{rve} \supset \Gamma^* \quad (3)$$

expressed in the relevant molecular symmetry (MS) group [74]. In Eq. (3), Γ_{e^-} is the symmetry of the photoelectron partial wave which in the asymptotic range reduces to its parity (+ for even ℓ partial waves and − for odd ℓ partial waves), Γ^* denotes the dipole moment representation of the relevant molecular symmetry group and Γ^+_{rve} and Γ''_{rve} stand for the rovibronic symmetries of the cationic and neutral states, respectively. Conservation of the total angular momentum $\vec{\mathbf{J}}$ upon ionization leads to the additional restriction for a single-photon excitation process [71]:

$$\Delta J = J^+ - J'' = -\ell - \frac{3}{2}, -\ell - \frac{1}{2}, \ldots, \ell + \frac{3}{2}, \quad (4)$$

where ℓ stands for the orbital angular momentum quantum number of the photoelectron partial wave and J'' and J^+ for the total angular momentum quantum numbers (excluding nuclear spins) of the neutral and cationic states, respectively.

The main advantage of the rotational selection rules derived from Eq. (3) for a given vibronic transition is their strict validity and their ease of implementation. They have successfully been applied to the analysis of the PFI-ZEKE photoelectron spectra of a number of polyatomic molecules such as ND_4 [75], NH_3 [76], C_6H_6 [73,77], C_6H_6-rare gas clusters [78], H_2O [73], CH_2CO [37,38], CH_2 [32], NH_2 [33] and C_2H_4 [39,40]. However, the drawback of these selection rules is that they provide only limited information on the photoionization dynamics (i.e., intensities) and primarily help to predict the even- or odd-ℓ nature of the photoelectron partial waves associated with a given rovibronic photoionization transition.

Up to date, several numerical models for the calculation of rovibronic photoionization intensities based on Eq. (2) have been described in the literature. They generally differ in the approximations that are introduced in the evaluation of Eq. (2). In their pioneering work on the theory of the rotational structure in photoelectron spectra of diatomic molecules, Buckingham et al. introduced a set of approximations to evaluate Eq. (2) which enabled the calculation of relative rovibrational intensities of photoelectron bands without the need to solve the scattering problem explicitly. When applied within the so-called orbital approximation [1], the model relates the rotational structure observed in photoelectron bands to the properties of the molecular orbital from

which the electron is ejected and thus provides a physically appealing interpretation of the photoionization dynamics already mentioned in the introduction. The original derivation was restricted to diatomic molecules and its extension to treat the photoionization of asymmetric tops [39,42] will be discussed in Section 3.

McKoy and co-workers developed a full ab initio treatment of Eq. (2) where the Lippmann–Schwinger scattering equation is solved numerically (see, e.g., [43,45–47]). The model has successfully been applied to analyze the rotational structure of the PFI-ZEKE photoelectron spectra of a variety of molecules such as N_2 [79], NO [80–82], CO [79], H_2O [23–25], HCl [57], OH [83,84], SH [85], HBr [86], H_2CO [34], CH_3 [34] and O_2 [87]. While providing a rather detailed and complete picture of the photoionization dynamics, such ab initio calculations are computationally demanding and do not enable simple predictions of the rotational structure of a photoelectron spectrum as are often needed by experimentalists in the assignment procedure of their spectra.

A recent approach to calculate the rotational structure of photoelectron spectra using Eq. (2) was introduced by Ford and Müller-Dethlefs [88,35] and is reminiscent of the orbital approximation of the BOS model but introduces different approximations in the evaluation of the electronic transition moment. The initial state of the photoionizing transition is treated as a Rydberg-like state on which the cationic state is projected. This projection is interpreted as a "spectator orbital" from which the photoelectron is removed. In some cases this approximation can be fairly accurate, in others less so because typical initial states of photoionization transitions in polyatomic molecules are usually valence states with little Rydberg character. The determination of the spectator orbital requires some initial knowledge of the cationic electronic structure, e.g., from an ab initio calculation. The physical interpretation of the photoionization dynamics that emerges from this treatment is quite similar to the one drawn from the orbital approximation of Ref. [1], namely that the rotational structure of the photoelectron bands can be related to the properties of the orbital from which the electron is removed which is in this case the spectator orbital.

3. Rotational line strengths in the photoelectron spectra of asymmetric-top molecules

The advantage of the orbital approximation lies in the fact that it provides an intuitive interpretation of the photoionization process and of the rotational intensity distribution in photoelectron spectra. It also represents a valuable aid in the rovibronic assignment of the spectral features and the determination of the vibronic symmetry of the cationic states. The original derivation was restricted to diatomic molecules and the generalization to asymmetric tops, detailed in Refs. [39,42] is briefly outlined here.

The electronic and vibrational angular momenta are not constants of motion in asymmetric-top molecules. In the absence of spins, or whenever the effects of spins can be neglected (which is often the case in asymmetric tops [89]), the total angular momentum without spin $\vec{\mathbf{N}}$ is used. The photoionization process can thus be treated as a transition from a Hund's case (b) to a Hund's case (d) type angular momentum coupling scheme [62]. For the evaluation of the electronic transition moment, it is assumed that (i) the electronic wavefunction can be described with a single Slater determinant, (ii) ionization occurs out of a single molecular orbital, and (iii) the molecular orbital structure does not change upon the removal of an electron. Under these assumptions, which are often referred to as the frozen-core Hartree-Fock approximation, the electronic transition moment reduces to a one-electron integral involving the molecular orbital $\phi_{\alpha''}$ from which ionization occurs and the photoelectron continuum orbital. This corresponds to the orbital approximation introduced in Ref. [1]. $\phi_{\alpha''}$ is decomposed into its angular momentum components in a single-center expansion in the molecular center of mass:

$$\phi_{\alpha''} = \sum_{|\lambda''|\leq \ell''}^{\infty} C^{(\alpha'')}_{\ell''\lambda''} R_{\alpha''\ell''}(r) Y_{\ell'',\lambda''}(\vartheta,\varphi), \tag{5}$$

with the expansion coefficients $C^{(\alpha'')}_{\ell''\lambda''}$, the radial functions $R_{\alpha''\ell''}(r)$ and the spherical harmonics $Y_{\ell'',\lambda''}(\vartheta,\varphi)$. α'' denotes the orbital index and ℓ'' and λ'' stand for the quantum numbers of the orbital angular momentum and its projection on the molecular axis, which is identified with the a or c inertial axis depending on whether the asymmetric top is near-prolate or near-oblate, respectively. The asymmetric-top wavefunctions $|NK_aK_c\rangle$ are expanded in a basis of symmetric-top functions $|NK\rangle$

$$|NK_aK_c\rangle = \sum_K c_K^{NK_aK_c} |NK\rangle \tag{6}$$

with the expansion coefficients $c_K^{NK_aK_c}$. In Eq. (6), K_a and K_c represent the asymmetric-top quantum numbers and K the quantum number of the projection of $\vec{\mathbf{N}}$ on the internuclear axis. With these approximations, the total ionization cross section σ at energy E is calculated to be [39,42]

$$\sigma_{\text{tot}} \propto \rho''|\langle v^+|v''\rangle|^2 \sum_{|\lambda''|\leq\ell''} \tfrac{1}{2\ell''+1} Q(\ell'') |C^{(\alpha'')}_{\ell''\lambda''}|^2 \left[\ell''|F^{E,\ell''-1}_{\alpha''\ell''}|^2 + (\ell''+1)|F^{E,\ell''+1}_{\alpha''\ell''}|^2\right]$$
$$\text{with} \quad Q(\ell'') = (2N^+ + 1)\left[\sum_{K^+K''} (-1)^{K^+} c^{N^+K_a^+K_c^+}_{K^+} c^{N''K_a''K_c''}_{K''} \begin{pmatrix} N^+ & \ell'' & N'' \\ -K^+ & \lambda'' & K'' \end{pmatrix}\right]^2. \tag{7}$$

In Eq. (7),

$$\rho'' = \chi'' \exp\left\{-\frac{E''}{k_B T}\right\}(2N''+1) \quad (8)$$

represents the weighting factor of the initial rovibronic level of the neutral state with spin-statistical weight χ'', and E'' represents the energy with respect to the lowest level. The vibrational part of the transition moment is contained in the factor $|\langle v^+|v''\rangle|^2$. $F^{E,\ell}_{\alpha''\ell''}$ represents a radial transition integral of the form

$$F^{E\ell}_{\alpha''\ell''} = \int_0^\infty R_\ell(E,r) R_{\alpha''\ell''}(r) r^3 \mathrm{d}r. \quad (9)$$

where $R_\ell(E,r)$ denotes the radial part of the photoelectron partial wave and ℓ its orbital angular momentum quantum number.

Eq. (7) allows a straightforward interpretation of the photoionization dynamics of asymmetric tops which can be inferred from the $3j$ symbol in the angular factor $Q(\ell'')$: the change of the rotational angular momentum $\vec{\mathbf{R}} \equiv \vec{\mathbf{N}}$ upon photoionization is caused by the angular momentum components (ℓ'', λ'') of the molecular orbital from which ionization occurs. In other words, the removal of an electron creates an orbital angular momentum "hole" which can couple to the rotational angular momentum and is responsible for the rotational fine structure observed in photoelectron bands. This physical picture, already illustrated in the introduction with the example of H_2, is a direct result of the orbital approximation and represents the salient feature of the model which can thus adequately be termed "orbital ionization model".

Eq. (7) also offers a means to reconstruct the angular momentum components (ℓ'', λ'') of the photoelectron from experimental data [48]. The $3j$ symbol in $Q(\ell'')$ is different from zero only if $|\Delta N| = |N^+ - N''| \leq \ell''$ and $\Delta K = K^+ - K'' = \lambda''$ hold. Hence, the maximum value of ℓ'' can be determined from the rotational transition with the maximum value of ΔN, and the different observed ΔK_a, ΔK_c components allow one to derive the relevant λ'' components of the single-center expansion using Eq. (6). Note that the condition $|\Delta N| \leq \ell''$ is more restrictive than the general expression Eq. (4).

Eq. (7) constitutes a complete, though approximate, rovibronic intensity model for the photoionization of asymmetric tops. The simulation of the rovibronic structure of photoelectron spectra can be performed if the vibrational factors $|\langle v^+|v''\rangle|^2$, the expansion coefficients of the single-center expansion $C^{(\alpha'')}_{\ell''\lambda''}$ and the radial transition integrals $F^{E\ell}_{\alpha''\ell''}$ are calculated, for instance with ab-initio methods. In many situations only a transition to a single cationic electronic state is considered and only the relative intensities of the rovibrational components are of interest. In this case, the vibrational intensities are determined by the factor $|\langle v^+|v''\rangle|^2$ which can in a first approximation be expressed as a Franck-Condon factor $\prod_i |\langle v_i^+|v_i''\rangle|^2$, where the product is over all normal modes i. An analysis of the relative rotational intensities of a particular vibronic band can be performed when the factors

$$B^{(\alpha'')}_{\ell''\lambda''} = |C^{(\alpha'')}_{\ell''\lambda''}|^2 [\ell''|F^{E,\ell''-1}_{n\ell''}|^2 + (\ell''+1)|F^{E,\ell''+1}_{n\ell''}|^2] \quad (10)$$

in Eq. (7) are treated as effective parameters which are fitted to the experimentally observed spectrum. Alternatively, if the single-center expansion coefficients $C^{(\alpha'')}_{\ell''\lambda''}$ are already known, the factors

$$b^{(\alpha'')}_{\ell''\lambda''} = [\ell''|F^{E,\ell''-1}_{n\ell''}|^2 + (\ell''+1)|F^{E,\ell''+1}_{n\ell''}|^2] \quad (11)$$

can be treated as adjustable parameters. In this way, Eq. (7) can be used as an empirical model for relative rotational photoionization intensities which allows one to extract valuable information on the photoionization dynamics from experimental data. The following procedure can be adopted for the interpretation of the rotational structure of photoelectron bands:

1. Assignment of the electronic symmetry and of the rotational transitions using the rotational selection rules derived from Eq. (3) and determination of the rotational energy levels.
2. Determination of the molecular constants (ionization energies, rotational constants, centrifugal distortion constants, etc.) by a fit to the experimentally determined line positions.
3. Determination of the different rotational branches of the photoelectron spectrum and hence of the angular momentum propensity rules.
4. Analysis of the valence orbitals of the neutral parent molecule and qualitative determination of their angular momentum components in the core region to provide an initial set of $B^{(\alpha'')}_{\ell''\lambda''}$ parameters and simulate the relative rotational spectral intensities using Eq. (7).
5. Iterative refinement of the $B^{(\alpha'')}_{\ell''\lambda''}$ parameters (and identification of possible systematic deviations) until agreement between simulated and observed spectra is achieved.

The simple physical picture of photoionization dynamics which is the result of the orbital ionization model is a direct consequence of the approximations introduced in the evaluation of the transition moment, i.e., the frozen-core Hartree-Fock approximation. Consequently, if the neutral, the cationic, or both states are subject to configuration interaction or if the molecular geometry changes significantly upon ionization, the vibronic intensities calculated using Eq. (7) will deviate from the observed ones: If additional electronic angular momentum components are introduced into the electronic wavefunction by configurational mixing, rotational transitions can be observed which are not compatible with the assumption that ionization occurs out of a single orbital. In this case, the configuration interaction can be detected on the basis of simulations using Eq. (7), and the deficiency of the model can be compensated by introducing suitable $B^{(\alpha'')}_{\ell''\lambda''}$ parameters to account for the additional angular momentum contributions. These parameters in turn provide informa-

tion on the configurations that are mixed in (see Section 5.4).

The main limitation of the model is that interactions between the photoelectron and the cationic core are not taken into account; the photoelectron merely acts as a "spectator" that is not influenced by the dynamics of the ionic core [12], the coupling between different ionization channels mediated by the electron–ion core interaction at short range being neglected. In PFI-ZEKE photoelectron spectroscopy, the effects of channel interactions on rovibrational intensity distributions are well documented [12] and primarily arise from the coupling of the pseudo-continua of high Rydberg states that are probed in a PFI-ZEKE experiment with lower Rydberg states belonging to different ionization channels. These channel interactions can also be viewed as resulting from the scattering of the Rydberg electron at the dipole or higher multipoles of the molecular core in the short-range region of the electron-ion collision [81,26,24] and typically lead to a change of the partial wave character of the photoelectron and to the appearance of additional rovibronic transitions in the spectra.

The importance of intensity perturbations caused by channel interactions tends to decrease with increasing size of the molecules and with increasing spectral resolution. The reasons are the short lifetimes and the resulting large resonance widths of low Rydberg states in larger polyatomics which cause channel interactions to average out in many cases and the fact that accidental degeneracies between low-n Rydberg states and the pseudocontinua of high Rydberg states become rare with decreasing width of the field-ionization window. Among the examples presented in Section 5, intensity perturbations induced by autoionization were found to play only a minor role except in the case of the triatomic hydrides [22,23,32,33], as will be discussed in Section 5.3.

4. Experimental

A variety of experimental techniques can be employed to achieve rotational resolution in PFI-ZEKE photoelectron spectra. The most direct approach is single-photon excitation from the vibronic ground state using tunable narrow-bandwidth vacuum-ultraviolet (VUV) or extreme-ultraviolet (XUV) radiation sources [90,91]. Whenever VUV sources are not available, resonant multiphoton excitation schemes are used (see, e.g., Ref. [88]). Resonant schemes rely on the existence of suitable intermediate states and offer the advantage of considerably reducing the rotational line density in the PFI-ZEKE photoelectron spectra by selecting a single rotational level in the first excitation step. The assignment of the spectra is thus facilitated and rotational resolution can often be achieved with light sources of moderate bandwidth such as pulsed dye lasers and synchrotrons, as has been demonstrated in recent studies using IR-VUV [40,92] and VUV-UV [93] $(1+1')$ excitation sequences. Moreover, it is also possible to take advantage of the different Franck-Condon factors for the ionization from the intermediate state compared to the ionization from the ground neutral state, as has been shown in a recent PFI-ZEKE photoelectron spectroscopic study on the $\tilde{X}^{+\,3}B_1$ ground state of NH_2^+ [94]. Alternatively, by keeping the ionization laser frequency fixed and tuning the frequency of the laser for the excitation to the intermediate state it is possible to record excitation spectra of selected species which have recently been used to study the rotational structures of conformers of polyatomic molecules [36].

The PFI-ZEKE photoelectron spectrometers and experimental procedures used in our investigations have been described in detail in previous publications [90,75,91,19]. Briefly, PFI-ZEKE photoelectron spectra are recorded by pulsed-field ionization of high Rydberg states [10] after single-photon excitation from the neutral ground vibronic state using broadly tunable vacuum-ultraviolet (VUV) radiation sources. The VUV radiation is generated by resonance-enhanced difference- or sum-frequency mixing in a Krypton or Xenon gas jet using either the output of two pulsed dye lasers [75,90] or two pulse-amplified cw ring dye lasers [91]. The bandwidths obtained in the VUV using these two different laser systems are 0.1 cm^{-1} and 0.008 cm^{-1}, respectively. The combination of these narrow-bandwidth laser systems with carefully designed sequences of electric field pulses for the pulsed field ionization allows PFI-ZEKE photoelectron spectra to be recorded at a spectral resolution of up to 0.06 cm^{-1} [19].

5. Applications of the orbital ionization model

5.1. Dependence of rotational line intensities on molecular orbital properties

A simple example illustrating the formalism discussed in Section 3 is the photoionization of ketene CH_2CO, a molecule of C_{2v} symmetry [37]. The PFI-ZEKE photoelectron spectrum of the $\tilde{X}^1A_1(0,0,0) \rightarrow \tilde{X}^{+2}B_1(0,0,0)$ photoelectron band of CH_2CO is displayed in Fig. 1(a). In this transition, the electron is removed from the highest occupied molecular orbital (HOMO) $2b_1$. Ketene is a near prolate asymmetric top (the asymmetry parameter is $\kappa'' = -0.997$) in which the A'' rotational constant ($A'' = 9.0988\,cm^{-1}$) is more than an order of magnitude larger than the B'' and C'' constants ($B'' = 0.34377\,cm^{-1}$, C''=0.33074 cm^{-1}) [95] so that only the $K_a'' = 0$ and 1 levels are appreciably populated in the low temperature environment of the supersonic expansion ($T_{rot} = 5\,K$). The large A'' and A^+ constants lead to the grouping of the lines into three distinct bands observed in Fig. 1(a) corresponding to the transitions $K_{aK_a''}^+ = 0_1$, 1_0 and 2_1 on which different ΔN branches are superimposed. Within the framework of our intensity model, it can be concluded from the observed branches ($|\Delta K_a| \approx |\Delta K| = 1$ and $|\Delta N| \leq 2$) that the single center expansion of the $2b_1$ orbital must be dominated by $(\ell'', \lambda'') = (1, \pm 1)$ and $(2, \pm 1)$ components. This is readily verified by inspection of the $2b_1$ orbital shown

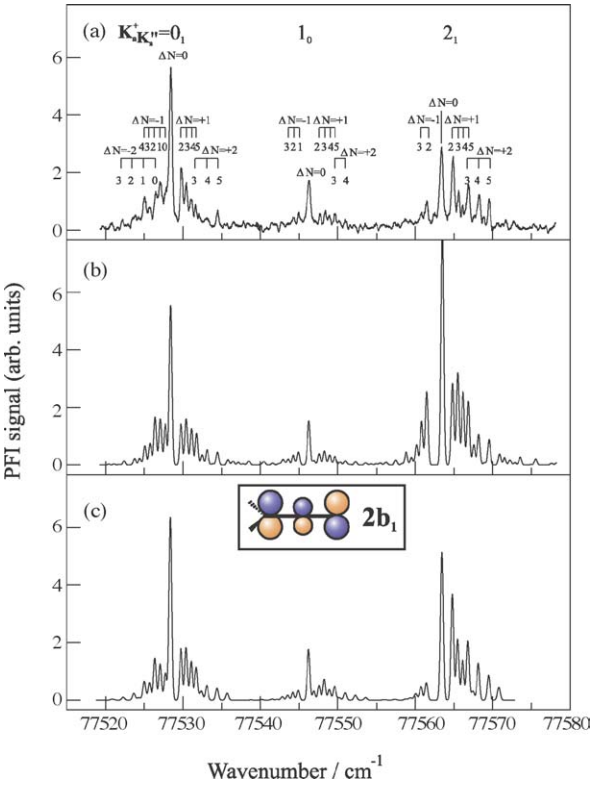

Fig. 1. (a) PFI-ZEKE photoelectron spectrum of the $\tilde{X}\,^1A_1(0,0,0) \rightarrow \tilde{X}^+\,^2B_1(0,0,0)$ photoelectron transition of ketene CH_2CO. The spectral branches are labeled by the asymmetric-top quantum numbers K_a in the neutral (") and cationic (+) states, respectively, using the notation $K^+_{aK_a''}$ and the changes in the total angular momentum without spin $\Delta N = N^+ - N''$. The values of N^+ are indicated below the assignment bars. (b) Simulation of the experimental spectrum using a simple model in which the line intensities are determined by the populations of the lower states and weighting coefficients for the rotational branches (see text). (c) Simulation of the experimental spectrum using the orbital ionization model. Inset: schematic representation of the highest occupied molecular orbital ($2b_1$) of CH_2CO.

in the inset in Fig. 1(c): The two outer p atomic orbitals form a contribution of $(\ell'', \lambda'') = (2, \pm 1)$ character and the central p atomic orbital is well described by an angular momentum component of (1,±1).

In Fig. 1(b), a simulation of the rotational structure based on a simple "Boltzmann" model is shown in which the relative rotational intensities are determined by the weights of the neutral states as expressed in Eq. (8). To reproduce the experimental spectrum, the relative intensities of the ΔN components were scaled according to the scheme $I(|\Delta N| + 1) = I(\Delta N)/3$. Although the overall intensity distribution is predicted quite satisfactorily with this crude model, the simulated spectrum deviates from the observed one in several details. The relative intensities of the $\Delta N = 0$ branches of the $K^+_{aK_a''} = 0_1$ and 2_1 bands are not simulated correctly, and neither are the ΔN=1 and 2 components of the $K^+_{aK_a''} = 2_1$ band. Fig. 1(c) shows a simulation of the spectrum using Eq. (7) assuming that the single-center expansion of the $2b_1$ molecular orbital consists of two dominant contributions $(\ell'', \lambda'') = (1, \pm 1)$ and $(2, \pm 1)$. The ratio of coefficients $|B^{(2b_1)}_{2,\pm1}:B^{(2b_1)}_{1,\pm1}| = 1 : 0.8$ was found to best reproduce the experimental spectrum. The agreement between the observed and experimental spectrum is quantitative; in particular details like the relative line intensities within the $\Delta N = +1$ and +2 branches of the $K^+_{aK_c''} = 2_1$ component are reproduced correctly.

5.2. Assigning the vibronic symmetry of photoelectron bands with the orbital ionization model

A more complicated case is found in the photoionization of ozone O_3 which also serves as an example to illustrate how the analysis of the photoionization dynamics can assist in the vibronic assignment of photoelectron bands. Ozone has been the subject of many theoretical and experimental investigations, and it has already been recognized in early ab-initio calculations that configuration interaction must be taken into account for a correct description of its ground state electronic wavefunction (see, e.g., Refs. [96–98]). Fig. 2 shows a schematic representation of the relevant molecular orbitals of O_3 together with the most important configurations contributing to the $\tilde{X}\,^1A_1$, $\tilde{X}^+\,^2A_1$ and $\tilde{A}^+\,^2B_2$ states as predicted by theory [98,41]. Because of configuration interaction, the $\tilde{X}^+$ state of O_3^+ is not formed by ionization out of the HOMO, the $1a_2$ orbital. Instead, the $\tilde{X}^+$ state wavefunction is dominated by the contribution from the $6a_1^{-1}$ ionization of the main neutral ground state configuration. Similarly, the leading configuration of the $\tilde{A}^+$ state wavefunction is predicted to arise from $4b_2^{-1}$ ionization (see Fig. 2). Studies by conventional photoelectron spectroscopy indicated that the first two cationic electronic states are almost degenerate [99,100]. However, the resolution achieved in these investigations was not sufficient in order to determine whether the ground state is the $^2A_1$ or the $^2B_2$ component. The experimental confirmation of the theoretical prediction that the $\tilde{X}^+$ state is of $^2A_1$ electronic symmetry [101–103] has only been achieved recently by the analysis of the rotational structure of the high-resolution PFI-ZEKE photoelectron spectrum which also showed that the origins of the $\tilde{X}^+$ and $\tilde{A}^+$ states are only separated by 1089.7 cm^{-1} [41]. This confirmation was performed on the basis of symmetry assignments and of simulations of the bands using the orbital ionization model.

The rotational structures of the origin bands of the $\tilde{X}\,^1A_1 \longrightarrow \tilde{X}^+\,^2A_1$ and $\tilde{X}\,^1A_1 \longrightarrow \tilde{A}^+\,^2B_2$ transitions are displayed in Fig. 3(a) and (b), respectively. Their rotational structures are very different because of the different rotational constants in the final state, the different selection rules caused by the different electronic symmetries of the cationic states and the differences in the photoionization dynamics. In a single-determinantal picture of the electronic wavefunction, the $\tilde{X}^+\,^2A_1$ state arises by ionization out of the $6a_1$ molecular orbital (see above). This orbital possesses a complex angular momentum composition as can be seen from its form depicted in Fig. 2. Consequently, the single-center expansion only converges slowly and a total of seven

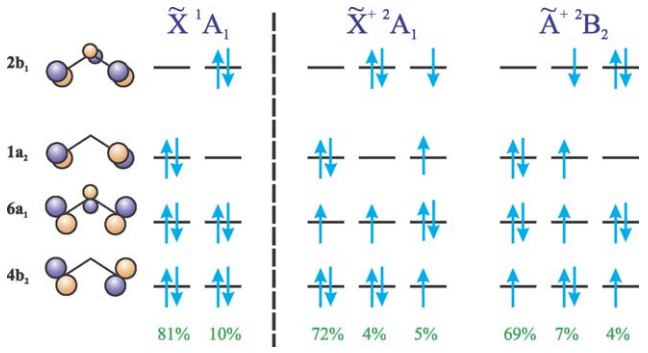

Fig. 2. Schematic representation of the outer valence molecular orbitals of ozone O_3 and dominant electronic configurations of the states $\tilde{X}\,^1A_1$, $\tilde{X}^+\,^2A_1$ and $\tilde{A}^+\,^2B_2$ (from Ref. [41]). The percentage numbers denote the relative contributions of the configurations to the CASSCF wavefunctions of these states.

angular momentum components $(\ell'', \lambda'') = (0, 0)$ (with coefficient $|B^{(6a_1)}_{0,0}| = 0.16$), (1,0) ($|B^{(6a_1)}_{1,0}| = 0.29$), (1,±1) ($|B^{(6a_1)}_{1,\pm1}| = 0.29$), (2,0) ($|B^{(6a_1)}_{2,0}| = 0.29$), (2,±1) ($|B^{(6a_1)}_{2,\pm1}| = 0.29$), (2,±2) ($|B^{(6a_1)}_{2,\pm2}| = 0.24$) and (3,±1) ($|B^{(6a_1)}_{3,\pm1}| = 0.29$) are needed in the simulation of the $\tilde{X}^+\,^2A_1(0, 0, 0)$ band (lower trace of Fig. 3(a)). Because of the high number of terms in the single-center expansion and the congestion of the experimental spectrum, the $B^{(\alpha'')}_{\ell''\lambda''}$ coefficients could only be determined with an accuracy of about 20%.

In contrast, the $\tilde{A}^+\,^2B_2$ state is formed by ionization out of the $4b_2$ orbital which shows a considerably simpler orbital angular momentum composition (see Fig. 2). The rotational intensity distribution of the $\tilde{A}^+\,^2B_2(0, 0, 0)$ band could be reproduced by assuming only two angular momentum components $(\ell'', \lambda'') = (1, 0)$ and $(2, \pm1)$ with equal weights (see bottom trace of Fig. 3(b)). The $(2, \pm1)$ component originates from the two outer p orbitals from which a distorted d-like orbital can be formed by adding a (1,0) component to account for the tilt of the p orbitals.

The fact that two different sets of $B^{(\alpha'')}_{\ell''\lambda''}$ coefficients must be used in the simulations of the two bands indicates clearly that the ionization occurs primarily out of two different orbitals and hence that two different electronic states are involved. The analysis of the photoionization dynamics turns out to be the key to the assignment of the rotational structure of these bands. The determination of the angular momentum composition of the ground state orbitals provides unambiguous information on the electronic assignment, namely that the ground ionic state is of $^2A_1$ and that the first excited electronic state is of $^2B_2$ symmetry.

5.3. Intensity perturbations

The intensity distribution of PFI-ZEKE photoelectron bands can be subject to perturbations caused by the interaction between different ionization channels, i.e., electronic, vibrational or rotational autoionization or predissociation [12]. A class of molecules the PFI-ZEKE photoelectron spectra of which are systematically influenced by channel interactions are the triatomic hydrides XH_2. The spectra of H_2O [20], CH_2 [32] and NH_2 [33] all show rotational transitions which are formally forbidden within an atomic picture of ionization. As an example, Fig. 4 shows the PFI-ZEKE photoelectron spectrum of the $\tilde{X}^2B_1(0, 0, 0) \longrightarrow \tilde{a}^+\,^1A_1(0, 0, 0)$ transition in NH_2. The $\tilde{a}^+\,^1A_1$ state of NH_2^+ arises by the removal of the single electron from the $1b_1$ molecular orbital of NH_2 which is a p orbital on the nitrogen atom and predominantly corresponds to a $(\ell'', \lambda'') = (1, \pm1)$ component in a single center expansion (see inset in Fig. 4). By applying the atomic selection rule $\ell = \ell'' \pm 1$, the photoelectron is expected to be

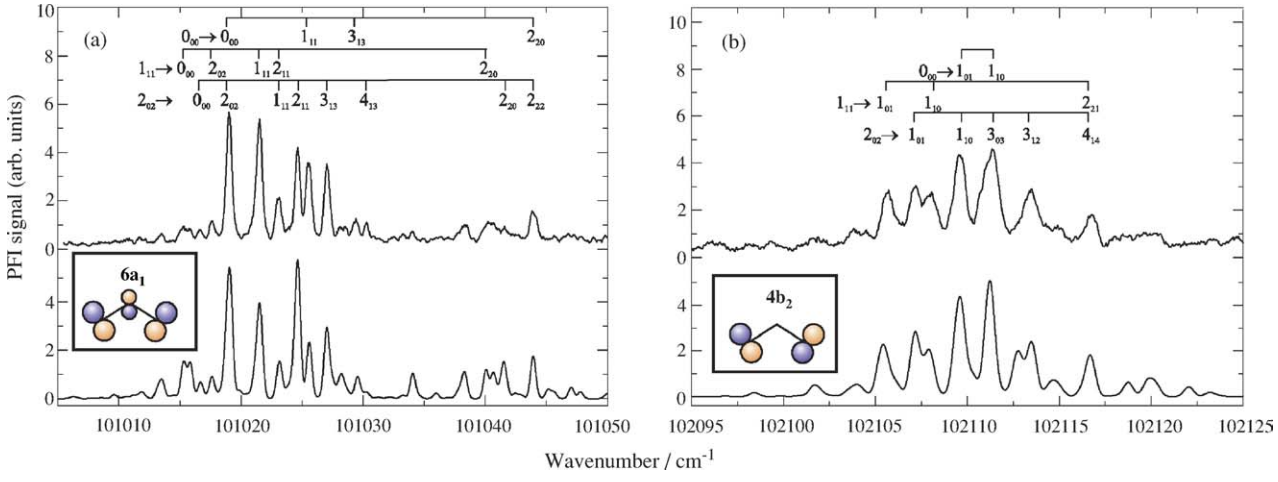

Fig. 3. *Upper traces:* PFI-ZEKE photoelectron spectra of (a) the $\tilde{X}\,^1A_1(0, 0, 0) \rightarrow \tilde{X}^+\,^2A_1(0, 0, 0)$ and (b) the $\tilde{X}\,^1A_1(0, 0, 0) \rightarrow \tilde{A}^+\,^2B_2(0, 0, 0)$ transitions of O_3. *Lower traces:* simulations using the orbital ionization model. The assignment bars indicate rotational transitions in the notation $N''_{K''_aK''_c} \rightarrow N^+_{K^+_aK^+_c}$. The differences in the observed rotational structures of the bands can be attributed to different rotational constants and selection rules as well as to the different molecular orbitals from which the photoelectron is ejected (insets). The analysis of the photoionization dynamics enables the unambiguous assignment of the cationic vibronic states of these transitions (adapted from Ref. [41].)

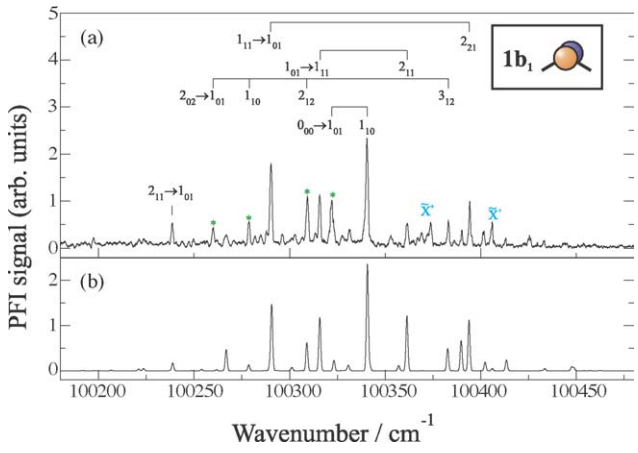

Fig. 4. (a) PFI-ZEKE photoelectron spectrum of the $\tilde{X}\,^2B_1(0,0,0) \longrightarrow \tilde{a}^+\,^1A_1(0,0,0)$ transition of NH_2. The assignment bars indicate rotational transitions in the notation $N''_{K''_a K''_c} \rightarrow N^+_{K^+_a K^+_c}$. The asterisks label "forbidden" rotational transitions associated with odd photoelectron partial wave components that arise by a rotational channel interaction. These channel interactions can be detected by a comparison with the simulated spectrum (b) which assumes ionization out of the $1b_1$ molecular orbital of NH_2 (inset) which corresponds to an almost pure $(\ell'', \lambda'') = (1, \pm 1)$ single-center orbital and hence only contains transitions associated with even photoelectron partial wave components. The lines labeled with "$\tilde{X}^+$" correspond to a transition to a highly excited bending level of $\tilde{X}^+\,^3B_1$ ground state of NH_2^+ (adapted from Ref. [33].)

ejected as a superposition of s and d partial waves. The simulation of the rotational intensities using the orbital ionization model (lower trace of Fig. 4) assumes ionization out of a $(\ell'', \lambda'') = (1, \pm 1)$ orbital and hence does not include the rotational transitions corresponding to odd-ℓ photoelectron waves. In this case, the rotational selection rules $\Delta K_a =$ odd and $\Delta K_c =$ even can be derived [33] and indeed, the majority of the rotational lines in Fig. 4 are found to obey these propensity rules.

However, a few transitions with $\Delta K_a =$ even and $\Delta K_c =$ odd can be observed (marked by asterisks in Fig. 4) which correspond to odd-ℓ photoelectron partial wave components and cannot be reconciled with ionization from a p-type orbital using the atomic selection rule $\ell = \ell'' \pm 1$. The odd parity of the partial-wave components associated with the "forbidden" transitions indicates an interaction of the photoelectron with odd moments of the ion core, primarily with the dipole. These transitions gain intensity by a rotational channel interaction that can be interpreted as a scattering of the Rydberg electron at the dipole moment of the cation core [22,26,24,33]. In this case, the differences between the simulated and experimental spectra enables one to detect intensity perturbations and to identify the corresponding channel interactions.

One should note that the "forbidden" transitions discussed above are allowed by the general rovibronic photoionization selection rules Eq. (3). In the case of H_2O, they were predicted by elaborate calculations as arising either from the interaction between ionization continua [23–26] or from the interaction between bound Rydberg states and ionization continua [22].

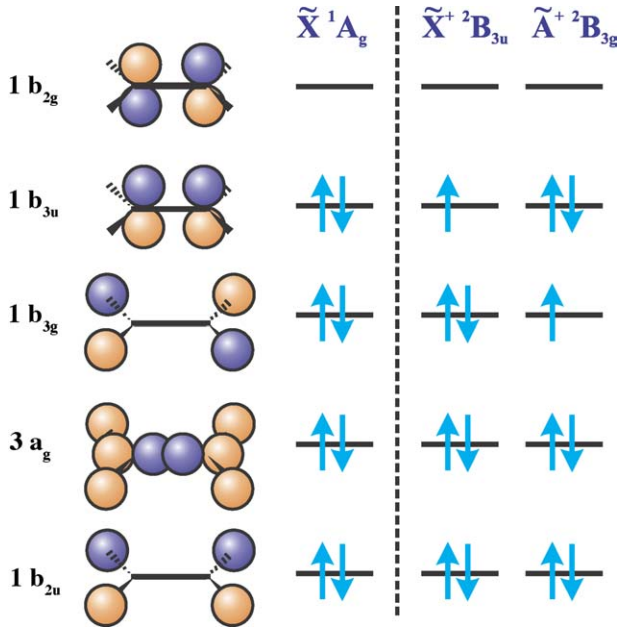

Fig. 5. Schematic representation of the outer valence molecular orbitals of ethylene C_2H_4 and configurations of the cationic states $\tilde{X}^+\,^2B_{3u}$ and $\tilde{A}^+\,^2B_{3g}$.

5.4. Studying the internal dynamics of the cation core using the orbital ionization model

Because the rovibronic structure of photoelectron bands depends on the properties of the molecular orbital from which ionization occurs, configuration interactions and vibronic interactions can strongly influence the photoionization dynamics. An illustrative example can be found in the photoionization of ethylene C_2H_4 [39]. Ethylene is the prototypical molecule exhibiting a double bond; it is a planar asymmetric top with D_{2h} symmetry. Its most important valence molecular orbitals are depicted in Fig. 5. The electronic ground state of $C_2H_4^+$ $\tilde{X}^+\,^2B_{3u}$ is formed by ionization out of the $1b_{3u}$ orbital. The $\tilde{X}\,^1A_g \longrightarrow \tilde{X}^+\,^2B_{3u}$ photoelectron band shows a long irregular progression in the torsional mode ν_4 which is indicative of a non-planar equilibrium geometry of the cationic ground state and a strongly anharmonic torsional potential (see Fig. 2 of Ref. [39]). An analysis of the vibrational progression revealed that the torsional motion in the $\tilde{X}^+$ state of $C_2H_4^+$ is governed by a double-well potential with a barrier of $\approx 360\,cm^{-1}$ at the planar geometry and that the lowest two states effectively constitute a tunneling pair [39]. This deviation from planarity of the molecule upon ionization can be explained by vibronic coupling with the first excited electronic state $\tilde{A}^+\,^2B_{3g}$ along the torsional coordinate [104,105]. This interaction also accounts for the observation of photoelectron bands with an odd number of torsional quanta in the cationic state (with vibrational symmetries $\Gamma_v^+ = A_u$) which are forbidden within the framework of the Franck-Condon approximation.

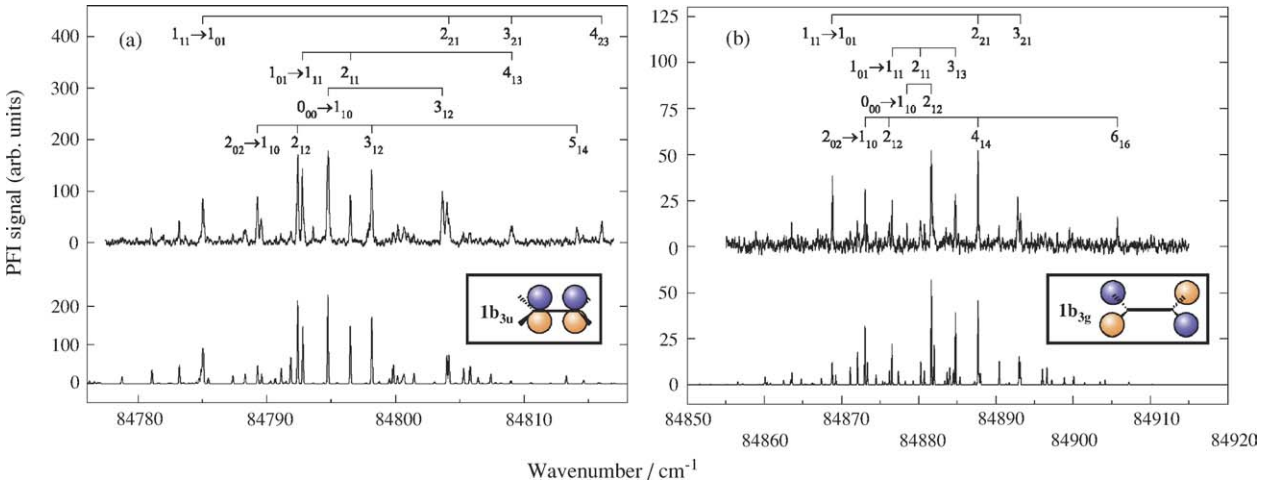

Fig. 6. PFI-ZEKE photoelectron spectra of the (a) $\tilde{X}\,^1A_g0^0 \rightarrow \tilde{X}^+\,^2B_{3u}0^0$ and (b) $\tilde{X}\,^1A_g0^0 \rightarrow \tilde{X}^+\,^2B_{3u}4^1$ transitions of C_2H_4. The transition to the 4^1 torsional level is forbidden within the Franck-Condon approximation and gains intensity by vibronic coupling to the $\tilde{A}^+\,^2B_{3g}$ electronic state of $C_2H_4^+$. The vibronic coupling is reflected by the rotational structure of the band. Insets: schematic representations of the molecular orbitals from which ionization occurs (adapted from Ref. [39].)

The high-resolution PFI-ZEKE photoelectron spectrum of the lowest two torsional bands 4^0 ($\Gamma_v^+ = A_g$) and 4^1 ($\Gamma_v^+ = A_u$) is presented in the upper traces of Fig. 6(a) and (b), respectively. The rotational structure of these two bands is different, although in both cases the same rotational selection rules ΔK_a = odd and ΔK_c = even hold [39]. The differences in the rotational intensity distribution can thus only be accounted for by an additional propensity rule which can be understood by considering the properties of the molecular orbitals from which ionization occurs. In the case of the 4^0 band, the electron is ejected from the $1b_{3u}$ orbital which predominantly corresponds to an $(\ell'', \lambda'') = (1, \pm1)$ orbital in a single-center expansion (see Fig. 5). The simulation of the spectrum using the orbital ionization model shown in the lower trace of Fig. 6(a) only contains this leading angular momentum contribution. In contrast, the rotational intensity distribution of the 4^1 band (shown in the upper trace of Fig. 6(b)) cannot be reconciled with ionization out of a (1,±1) single-center orbital. Instead, a simulation assuming that the photoelectron is ejected out of a (2,±1) single-center orbital gives good agreement with the observed spectrum (lower trace of Fig. 6(b)). This angular momentum composition is the unambiguous characteristic of the $1b_{3g}$ molecular orbital from which ionization to the $\tilde{A}^+\,^2B_{3g}$ state of the cation occurs (see Fig. 5). The photoionization dynamics thus indicates that the bands with an odd number of torsional quanta in the cationic state gain intensity by vibronic coupling to the $\tilde{A}^+\,^2B_{3g}$ state along the torsional coordinate. (Deviation from planarity leads to a mixing of the $1b_{3g}$ and $1b_{3u}$ orbitals because the molecule loses its inversion center.) The differences in the rotational intensity distributions for the 4^0 and 4^1 bands can therefore easily be explained with the orbital ionization model: they are caused by the different values of the 3j symbol in Eq. (7) for the $(\ell'', \lambda'') = (1, \pm1)$ and $(2, \pm1)$ single-center orbitals.

6. Conclusions

Recent progress in the experimental and theoretical study of the rovibronic photoionization dynamics of asymmetric-top molecules was reviewed. High-resolution PFI-ZEKE photoelectron spectra of CH_2CO, O_3, NH_2 and C_2H_4 were analyzed in terms of a theoretical model for rovibronic photoionization intensities of asymmetric tops which is based on a previous model for diatomic molecules developed by Buckingham et al. [1]. It was demonstrated that the rotational structure of photoelectron bands contains important information on the photoionization dynamics of the molecule. The good agreement between the experimentally observed and theoretically predicted rotational intensity distributions confirms the physical interpretation of the photoionization dynamics in terms of the molecular orbital from which ionization occurs.

This picture does not only provide a physically straightforward interpretation of the rotational structure of photoelectron spectra of a wide range of molecules for which the ionization dynamics can be described in a single-determinantal approximation, but it also provides a framework in which more complex situations can be discussed. First, the close relationship between the rotational structure observed in the photoelectron bands and the electronic structure of a molecule can be used to aid in the assignment of the vibronic symmetry of photoelectron bands as illustrated in Section 5.2 with the example of O_3. Second, a comparison between the experimental photoelectron spectra and spectra simulated on the basis of the orbital approximation allows one to detect intensity perturbations caused by interactions between different ionization channels (see Section 5.3). Third, the model can be used to identify vibronic interactions in the cation, and, in favorable cases such as C_2H_4 (Section 5.4), to unambiguously detect intensity anomalies caused by vibronic coupling in the cation.

The present formalism is not only applicable to the analysis of single-photon PFI-ZEKE photoelectron spectra, mass-analyzed threshold-ionization (MATI) spectra [106] and conventional photoelectron spectra, but can also be used in the context of resonant multi-photon ionization (REMPI) schemes. In this case, the rotational intensity distributions of the photoelectron bands reflect the angular momentum structure of the intermediate state.

The present results demonstrate that a detailed understanding of the photoionization dynamics of larger asymmetric tops can be reached by the resolution and the analysis of the rotational structure of the photoelectron bands. To study the photoionization dynamics of even larger molecules, new spectroscopic methods which allow a further increase in resolution such as cross-correlation ionization energy (CRIE) spectroscopy [107] or Rydberg-state-resolved threshold-ionization (RSR-TI) spectroscopy [108,76] will prove useful.

Acknowledgments

We gratefully acknowledge many useful discussions on the rotational structure of photoelectron spectra with Prof. T.P. Softley (Oxford) and Prof. R. Signorell (Göttingen). This work is supported financially by ETH Zürich and the Swiss National Science Foundation. SW thanks Christ Church (Oxford) for a Junior Research Fellowship.

References

[1] A.D. Buckingham, B.J. Orr, J.M. Sichel, Phil. Trans. R. Soc. London A 268 (1970) 147.
[2] D.W. Turner, C. Baker, A.D. Baker, C.R. Brundle, Molecular Photoelectron Spectroscopy. A Handbook of He 584 ÅSpectra, Wiley-Interscience, London, 1970.
[3] J. Berkowitz, Photoabsorption, Photoionization and Photoelectron Spectroscopy, Academic Press, New York, 1979.
[4] K. Kimura, S. Katsumata, Y. Achiba, T. Yamazaki, S. Iwata, Handbook of HeI Photoelectron Spectra of Fundamental Organic Molecules, Japan Scientific Societies Press, Tokyo, 1981.
[5] M.E. Russell, W.A. Chupka, J. Phys. Chem. 75 (1971) 3797.
[6] R.J.S. Morrison, W.E. Conaway, T. Ebata, R.N. Zare, J. Chem. Phys. 84 (1986) 5527.
[7] S.L. Anderson, Adv. Chem. Phys. 82 (1992) 177.
[8] P.M. Guyon, C. Alcaraz, Proc. SPIE 1858 (1993) 398.
[9] S.R. Mackenzie, T.P. Softley, J. Chem. Phys. 101 (1994) 10609.
[10] G. Reiser, W. Habenicht, K. Müller-Dethlefs, E.W. Schlag, Chem. Phys. Lett. 152 (1988) 119.
[11] K. Müller-Dethlefs, E.W. Schlag, Annu. Rev. Phys. Chem. 42 (1991) 109.
[12] F. Merkt, T.P. Softley, Int. Rev. Phys. Chem. 12 (1993) 205.
[13] F. Merkt, Annu. Rev. Phys. Chem. 48 (1997) 675.
[14] A. Held, E.W. Schlag, Acc. Chem. Res. 31 (1998) 467.
[15] R.C. Shiell, T.G. Wright, Annu. Rep. Prog. Chem., Sect. C 98 (2002) 375.
[16] I. Fischer, Int. J. Mass. Spectrom. 216 (2002) 131.
[17] T.P. Softley, Int. Rev. Phys. Chem. 23 (2004) 1.
[18] D.W. Turner, M.I. Al-Jobory, J. Chem. Phys. 37 (1962) 3007.
[19] U. Hollenstein, R. Seiler, H. Schmutz, M. Andrist, F. Merkt, J. Chem. Phys. 115 (2001) 5461.
[20] R.G. Tonkyn, R. Wiedmann, E.R. Grant, M.G. White, J. Chem. Phys. 95 (1991) 7033.
[21] F. Merkt, R. Signorell, H. Palm, A. Osterwalder, M. Sommavilla, Mol. Phys. 95 (1998) 1045.
[22] R.D. Gilbert, M.S. Child, Chem. Phys. Lett. 287 (1991) 153.
[23] M.-T. Lee, K. Wang, V. McKoy, J. Chem. Phys. 97 (1992) 3108.
[24] M.-T. Lee, K. Wang, V. McKoy, L.E. Machado, J. Chem. Phys. 97 (1992) 3905.
[25] M.-T. Lee, K. Wang, V. McKoy, J. Chem. Phys. 97 (1992) 3108.
[26] M.-T. Lee, K. Wang, V. McKoy, R.G. Tonkyn, R.T. Wiedmann, E.R. Grant, M.G. White, J. Chem. Phys. 96 (1992) 7848.
[27] W.L. Glab, P.T. Glynn, P.M. Dehmer, J.L. Dehmer, K. Wang, B.V. McKoy, J. Chem. Phys. 106 (1997) 5779.
[28] I. Fischer, A. Lochschmidt, A. Strobel, G. Niedner-Schatteburg, K. Müller-Dethlefs, V.E. Bondybey, J. Chem. Phys. 98 (1993) 3592.
[29] K. Wang, M.-T. Lee, V. McKoy, R.T. Wiedmann, M.G. White, Chem. Phys. Lett. 219 (1994) 397.
[30] I. Fischer, R. Lindner, K. Müller-Dethlefs, J. Chem. Soc. Faraday Trans. 90 (1994) 2425.
[31] S. Willitsch, L. Imbach, F. Merkt, J. Chem. Phys. 117 (2002) 1939.
[32] S. Willitsch, F. Merkt, J. Chem. Phys. 118 (2003) 2235.
[33] S. Willitsch, J.M. Dyke, F. Merkt, Mol. Phys. 102 (2004) 1543.
[34] R.T. Wiedmann, M.G. White, K. Wang, V. McKoy, J. Chem. Phys. 100 (1994) 4738.
[35] M.S. Ford, K. Müller-Dethlefs, Phys. Chem. Chem. Phys. 6 (2004) 23.
[36] M.S. Ford, X. Tong, C.E.H. Dessent, K. Müller-Dethlefs, J. Chem. Phys. 119 (2003) 12914.
[37] S. Willitsch, A. Haldi, F. Merkt, Chem. Phys. Lett. 353 (2002) 167.
[38] S. Wang, Y. Shi, Z.J. Jakubek, M. Barnett, B. Simard, K. Müller-Dethlefs, C.-P. Liu, Y.-P. Lee, J. Chem. Phys. 117 (2002) 6546.
[39] S. Willitsch, U. Hollenstein, F. Merkt, J. Chem. Phys. 120 (2004) 1761.
[40] P. Wang, X. Xing, S.J. Baek, C.Y. Ng, J. Phys. Chem. A 108 (2004) 10035.
[41] S. Willitsch, F. Innocenti, J.M. Dyke, F. Merkt, J. Chem. Phys. 122 (2005) 024311.
[42] S. Willitsch, Eidgenössische Technische Hochschule, Ph.D. thesis, Zürich, Diss ETH Nr. 15713, 2004.
[43] G. Raseev, H. Le Rouzo, H. Lefebvre-Brion, J. Chem. Phys. 72 (1980) 5701.
[44] R.R. Lucchese, D.K. Watson, V. McKoy, Phys. Rev. A 22 (1980) 421.
[45] R.R. Lucchese, G. Raseev, V. McKoy, Phys. Rev. A 25 (1982) 2572.
[46] K. Wang, V. McKoy, I. Powis, T. Baer, C.Y. Ng (Eds.), High Resolution Laser Photoionization and Photoelectron Studies, John Wiley & Sons, Chichester, 1995, pp. 281–329.
[47] H. Lefebvre-Brion, G. Raseev, Mol. Phys. 101 (2003) 151.
[48] J.M. Sichel, Mol. Phys. 18 (1970) 95.
[49] L. Åsbrink, Chem. Phys. Lett. 7 (1970) 549.
[50] F. Merkt, T.P. Softley, J. Chem. Phys. 96 (1992) 4149.
[51] S. Stimson, Y.J. Chen, M. Evans, C.L. Liao, C.Y. Ng, C.W. Hsu, P. Heimann, Chem. Phys. Lett. 289 (1998) 507.
[52] A. Lafosse, M. Lebech, J.C. Brenot, P.M. Guyon, L. Spielberger, O. Jagutzki, J.C. Houver, D. Dowek, J. Phys. B: At. Mol. Opt. Phys. 36 (2003) 4683.
[53] J.L. Dehmer, D. Dill, J. Chem. Phys. 65 (1976) 5327.
[54] J.W. Cooper, Phys. Rev. 128 (1962) 681.
[55] G.R. Farquar, J.S. Miller, E.D. Poliakoff, K. Wang, V. McKoy, J. Chem. Phys. 115 (2001) 9764.
[56] H. Rudolph, V. McKoy, J. Chem. Phys. 91 (1989) 7995.
[57] K. Wang, V. McKoy, J. Chem. Phys. 95 (1991) 8718.
[58] T.F. Gallagher, Rydberg Atoms, Cambridge University Press, Cambridge, 1994.

[59] S. Fredin, D. Gauyacq, M. Horani, Ch. Jungen, G. Lefevre, Mol. Phys. 60 (1987) 825.
[60] T.P. Softley, A.J. Hudson, R. Watson, J. Chem. Phys. 106 (1997) 1041.
[61] Ch. Jungen (Ed.), Molecular Applications of Quantum Defect Theory, Institute of Physics Publishing, Bristol, Philadelphia, 1996.
[62] M.S. Child, Ch. Jungen, J. Chem. Phys. 93 (1990) 7756.
[63] A. Osterwalder, A. Wüest, F. Merkt, Ch. Jungen, J. Chem. Phys. 121 (2004) 11810.
[64] H. Dickinson, T. Chelmick, T.P. Softley, Chem. Phys. Lett. 338 (2001) 37.
[65] H.A. Bethe, E.E. Salpeter, Quantum Mechanics of One- and Two-Electron Atoms, Springer, Berlin, 1957.
[66] S.N. Dixit, V. McKoy, J. Chem. Phys. 82 (1985) 3546.
[67] D.J. Leahy, K.L. Reid, R.N. Zare, J. Chem. Phys. 95 (1991) 1757.
[68] H. Park, R.N. Zare, J. Chem. Phys. 104 (1996) 4568.
[69] D. Townsend, K.L. Reid, J. Chem. Phys. 112 (2000) 9783.
[70] S.N. Dixit, V. McKoy, Chem. Phys. Lett. 128 (1986) 49.
[71] J. Xie, R.N. Zare, J. Chem. Phys. 93 (1990) 3033.
[72] K. Müller-Dethlefs, J. Chem. Phys. 95 (1991) 4821.
[73] R. Signorell, F. Merkt, Mol. Phys. 92 (1997) 793.
[74] P.R. Bunker, P. Jensen, Molecular Symmetry and Spectroscopy, second ed., NRC Research Press, Ottawa, 1998.
[75] R. Signorell, H. Palm, F. Merkt, J. Chem. Phys. 106 (1997) 6523.
[76] R. Seiler, U. Hollenstein, T.P. Softley, F. Merkt, J. Chem. Phys. 118 (2003) 10024.
[77] K. Siglow, H.J. Neusser, J. Electron Spectrosc. Relat. Phenom. 112 (2000) 199.
[78] K. Siglow, H.J. Neusser, Faraday Discuss. 115 (2000) 245.
[79] W. Kong, D. Rodgers, J.W. Hepburn, K. Wang, V. McKoy, J. Chem. Phys. 99 (1993) 3159.
[80] S.N. Dixit, D.L. Lynch, V. McKoy, W.M. Huo, Phys. Rev. A 32 (1985) 1267.
[81] H. Rudolph, S.N. Dixit, V. McKoy, W.M. Huo, J. Chem. Phys. 88 (1988) 1516.
[82] H. Rudolph, S.N. Dixit, V. McKoy, W.M. Huo, J. Chem. Phys. 88 (1988) 637.
[83] R.T. Wiedmann, R.G. Tonkyn, M.G. White, K. Wang, V. McKoy, J. Chem. Phys. 97 (1992) 768.
[84] E. de Beer, C.A. de Lange, J.A. Stephens, K. Wang, V. McKoy, J. Chem. Phys. 95 (1991) 714.
[85] J.B. Milan, W.J. Buma, C.A. de Lange, K. Wang, V. McKoy, J. Chem. Phys. 107 (1997) 2782.
[86] N.L. Wales, W.J. Buma, C.A. de Lange, H. Lefebvre-Brion, K. Wang, V. McKoy, J. Chem. Phys. 104 (1996) 4911.
[87] M. Braunstein, V. McKoy, S.N. Dixit, J. Chem. Phys. 96 (1992) 5726.
[88] M. Ford, R. Lindner, K. Müller-Dethlefs, Mol. Phys. 101 (2003) 705.
[89] G. Herzberg, Molecular Spectra and Molecular Structure, vol. III, Electronic Spectra and Electronic Structure of Polyatomic Molecules, Krieger, Malabar, 1991.
[90] F. Merkt, A. Osterwalder, R. Seiler, R. Signorell, H. Palm, H. Schmutz, R. Gunzinger, J. Phys. B: At. Mol. Opt. Phys. 31 (1998) 1705.
[91] U. Hollenstein, H. Palm, F. Merkt, Rev. Sci. Instrum. 71 (2000) 4023.
[92] C.Y. Ng, J. Electron Spectrosc. Relat. Phenom. 142 (2005) 179.
[93] P. Rupper, F. Merkt, J. Chem. Phys. 117 (2002) 4264.
[94] S. Willitsch, F. Merkt, in press.
[95] L. Nemes, D. Luckhaus, M. Quack, J.W.C. Johns, J. Mol. Struct. 517 (2000) 217.
[96] P.J. Hay, T.H. Dunning, W.A. Goddard, J. Chem. Phys. 62 (1975) 3912.
[97] P. Borowski, K. Andersson, P.-A. Malmqvist, B.O. Roos, J. Chem. Phys. 97 (1992) 5568.
[98] R. Siebert, P. Fleurat-Lessard, R. Schinke, M. Bittererová, S.C. Farantos, J. Chem. Phys. 116 (2002) 9749.
[99] J.M. Dyke, L. Golob, N. Jonathan, A. Morris, M. Okuda, J. Chem. Soc. Faraday Trans. 70 (1974) 1828.
[100] S. Katsumata, H. Shiromaru, T. Kimura, Bull. Chem. Soc. Jpn. 57 (1984) 1784.
[101] N. Kosugi, H. Kuroda, S. Iwata, Chem. Phys. 58 (1981) 267.
[102] P. Decleva, D. De Alti, A. Lisini, J. Chem. Phys. 89 (1988) 367.
[103] T. Schmelz, G. Chambaud, P. Rosmus, H. Köppel, L. Cederbaum, H.-J. Werner, Chem. Phys. Lett. 183 (1991) 209.
[104] H. Köppel, W. Domcke, L.S. Cederbaum, W. von Niessen, J. Chem. Phys. 69 (1978) 4252.
[105] H. Köppel, L.S. Cederbaum, W. Domcke, S.S. Shaik, Angew. Chem. (Int. Ed. Engl.) 22 (1983) 210.
[106] L. Zhu, P.M. Johnson, J. Chem. Phys. 94 (1991) 5769.
[107] R.G. Neuhauser, K. Siglow, H.J. Neusser, J. Chem. Phys. 106 (1997) 896.
[108] R. Seiler, U. Hollenstein, G.M. Greetham, F. Merkt, Chem. Phys. Lett. 346 (2001) 201.